In-line microfluidic refractometer based on C-shaped fiber assisted photonic crystal fiber Sagnac interferometer

Chuang Wu,[1,2] Ming-Leung Vincent Tse,[2] Zhengyong Liu,[2] Bai-Ou Guan,[1,*] Chao Lu,[3] and Hwa-Yaw Tam[2]

[1]*Institute of Photonics Technology, Jinan University, Guangzhou 510632, China*

[2]*Department of Electrical Engineering, The Hong Kong Polytechnic University, Kowloon, Hong Kong, China*

[3]*Department of Electronic and Information Engineering, The Hong Kong Polytechnic University, Kowloon, Hong Kong, China*

**Corresponding author: tguanbo@jnu.edu.cn*

Received June 10, 2013; revised July 21, 2013; accepted July 24, 2013;
posted July 25, 2013 (Doc. ID 192057); published August 22, 2013

We propose and demonstrate a highly sensitive in-line photonic crystal fiber (PCF) microfluidic refractometer. Ultrathin C-shaped fibers are spliced in-between the PCF and standard single-mode fibers. The C-shaped fibers provide openings for liquid to flow in and out of the PCF. Based on a Sagnac interferometer, the refractive index (RI) response of the device is investigated theoretically and experimentally. A high sensitivity of 6621 nm/RIU for liquid RI from 1.330 to 1.333 is achieved in the experiment, which agrees well with the theoretical analysis. © 2013 Optical Society of America

OCIS codes: (060.2370) Fiber optics sensors; (060.5295) Photonic crystal fibers; (120.5790) Sagnac effect.
http://dx.doi.org/10.1364/OL.38.003283

Optical fibers are attractive candidates for the realization of optical biosensors since they are small in size, inexpensive to mass produce, and easy for signal delivery. In recent years, fiber-optic biosensors based on the measurement of induced refractive index (RI) change have received considerable attention [1]. For instance, long period fiber gratings (LPGs) have been proposed for biochemical sensing applications by utilizing their inherent characteristics of sensitivity to environmental RI changes [2]. Acid-etched fiber Bragg gratings (FBGs) have also been demonstrated as RI sensors for biosensing applications [3]. However, the sensitivities of LPG- and FBG-based RI sensors are usually no better than several hundred nanometers per refractive index unit (RIU). Further improvement of RI sensor's sensitivity is needed for detection of smaller concentration of molecules.

In the last few years, photonic crystal fiber (PCF)-based microfluidic refractometers have attracted great research attention because they exhibit extremely high sensitivity and the capability to detect analytes in very small volume (down to nL) [4,5]. The micrometer-sized air holes of PCFs are perfect microfluidic channels that allow gas/liquid to pass through. The optical properties of PCFs, such as transmission loss, birefringence, and dispersion, are highly dependent on the RI of the fluids filled in the air hole channels of the PCF. These enabled a lot of novel microfluidic RI sensors, e.g., absorption-based evanescent-wave sensors [6–9], FBGs in different types of PCFs [10], LPG in a large-mode-area PCF [11], selective-filling based PCF directional coupler sensor [12]. By filling the analytes into the air holes of a PCF-LPG, Rindorf and Bang achieved a RI sensitivity of 1460 nm/RIU, which is one order of magnitude higher than conventional LPGs [11]. Based on the coupling of the core mode to a nearby analyte-filled rod waveguide mode, an ultrahigh RI sensitivity of 30100 nm/RIU was demonstrated by Wu *et al.*, but it is limited to measure analytes with RI larger than that of silica [12].

There are mainly two approaches to couple light into and out of PCFs after liquid filling [6–12]. One is to directly splice the PCFs and the standard single-mode fiber (SMF); the other is based on free-space coupling. For the former, it is difficult to reuse the senor; for the latter, the use of adjustable stages and bulk optics makes the system complicated. In order to realize in-line access to the air holes of the PCFs, Cordeiro *et al.* demonstrated drilling holes on the side of PCFs by using the femtosecond laser micromachining technique [13]. However, it requires high-quality femtosecond laser beams and accurate positioning devices, rendering the device very expensive to produce.

In this Letter, we propose and demonstrate a high-sensitivity in-line PCF microfluidic RI sensor. Both ends of the PCF are low-loss connected to standard SMF through a thin piece of C-shaped fiber spliced in-between, which provide openings for liquids to flow in and out. The entire fabrication process only involves fusion splicing, hence it is potentially cost-effective. Based on a Sagnac interferometer, the RI response of the device is investigated theoretically and experimentally. A high sensitivity of 6621 nm/RIU for RI from 1.330 to 1.333 is achieved in the experiment, which agrees well with the theoretical analysis.

High-birefringence fiber loop mirror, also known as Sagnac interferometer, has been widely studied for sensing and WDM applications [14–17]. It consists of a broadband light source, an optical spectrum analyzer (OSA), and a 3 dB coupler with its two other arms connected with a piece of high-birefringence fiber, forming a closed Sagnac loop, as shown in Fig. 1(a). A polarization controller is also inserted in the loop to adjust polarization states and thus optimize interference intensity contrast. In such a Sagnac loop, the two counterpropagating light waves split by the 3 dB coupler recombine at the output port of the coupler, resulting in an interference spectrum that is relative to the phase difference between the two orthogonal modes guided in the high-birefringence fiber.

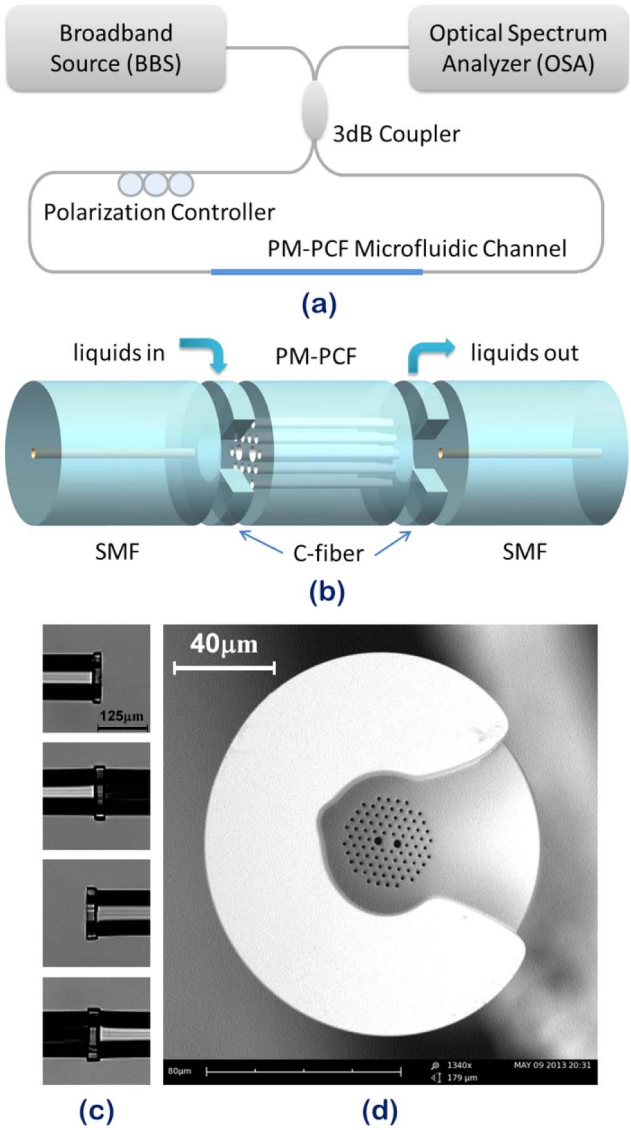

Fig. 1. (a) Schematic of the experimental setup. (b) Schematic of the fabricated SMF-C-PCF-C-SMF microfluidic structure. (c) Fabrication process of the microfluidic structure. (d) SEM photo of the PM-PCF with a thin cap of 20 μm thick C-shaped fiber.

In the experiment, a piece of polarization-maintaining (PM)-PCF (PM-1550-01, NKT Photonics) with length of 11.5 cm incorporated with two ultrathin pieces of C-shaped fiber on its both ends was used as the microfluidic RI sensing element, as shown in Fig. 1(b). Measured from a scanning electron microscope (SEM) photo of the PM-PCF, we find that the diameter of the small air holes is 2.25 μm and the pitch is 4.33 μm; the large air hole near the fiber core is slightly elliptical with a diameter of 4.20 μm × 4.60 μm. All the simulations presented hereinafter are based on the above geometrical parameters. The C-shaped fiber was fabricated in Photonics Research Center, Hong Kong Polytechnic University. A pure silica tube with an inner diameter of 4 mm and outer diameter of 12 mm is machined to create a lateral slot along the axial direction, resulting in a C-shaped preform. Then the preform is drawn into a C-shaped fiber with an outer diameter of 145 μm and inner diameter of 48 μm, so that the inner hollow area can cover the entire air-hole region of the PM-PCF. The fiber was drawn at a relatively low temperature of 1890°C to maintain the cross-sectional shape.

To fabricate the microfluidic device shown in Fig. 1(b), we first splice one SMF with a piece of C-shaped fiber, and then cut the C-shaped fiber to ~20 μm with the help of a microscope with 100 times amplification. The resultant SMF-C structure is shown in the top of Fig. 1(c). Since the C-shaped fiber is noncircular, manual splicing is needed. Next, the PM-PCF was spliced to another SMF with relatively low loss. After that, the SMF-C and the PCF-SMF portions are manually spliced together with the help of a tunable laser and a power meter to monitor the transmission loss during alignment, as shown in the second photo of Fig. 1(c). This step is the key part of the whole fabrication process because it is crucial to create an SMF-C-PCF joint with low loss, good strength, and without collapsing of the air holes of the PM-PCF. Dissatisfying any of the above three demands would lead to failure of the device. The splicing parameters including arc discharge intensity, duration/times, and position are optimized according to the method given in [18]. After the first SMF-C-PCF joint is made, we break the previous PCF-SMF joint and insert a thin piece of C-shaped fiber between them as previously done. Finally, an SMF-C-PCF-C-SMF microfluidic structure is achieved. The typical transmission loss of the entire structure is around 8 dB. The fusion splicer used is a FITEL S177A splicer.

Figure 1(d) shows the SEM photo of the end-view of the PM-PCF with a 20 μm thick C-shaped fiber attached. The mechanical strength is good, allowing the C-shaped fiber to be cut near the splicing point without breaking it. All the air holes of the PM-PCF are still open after fusion splicing. The liquid analytes can flow into the microfluidic channels of the PM-PCF through the side-opening "mouth" of the C-shaped fiber, as illustrated in Fig. 1(b). We insert the fabricated SMF-C-PCF-C-SMF structure into the fiber loop mirror shown in Fig. 1(a), and an in-line microfluidic Sagnac interferometer is constructed.

The transmission spectrum of Sagnac interferometer is approximately equal to a periodic function of wavelength and can be expressed by [14]

$$T = \frac{1}{2}\left[1 - \cos\frac{2\pi B(\lambda, n_a)L}{\lambda}\right], \tag{1}$$

where λ is the free-space wavelength, n_a is the RI of the analyte filled in the air hole channels of the PM-PCF, and L is the length of the PM-PCF. The phase modal birefringence B and group modal birefringence G of the PM-PCF are defined by

$$B(\lambda) = n_{\text{eff}}^{\text{slow}}(\lambda) - n_{\text{eff}}^{\text{fast}}(\lambda); \qquad G(\lambda) = B(\lambda) - \lambda\frac{dB(\lambda)}{d\lambda}, \tag{2}$$

where $n_{\text{eff}}^{\text{slow}}(\lambda)$ and $n_{\text{eff}}^{\text{fast}}(\lambda)$ are the effective indices of the two linear polarized modes of the PM-PCF. Transmission dips appear when the phase difference satisfies

$$\frac{2\pi B(\lambda, n_a)L}{\lambda} = 2m\pi, \tag{3}$$

where m is an integer. In order to deduce the RI sensitivity of our microfluidic Sagnac interferometer, we calculate the derivative of two sides of Eq. (3) with respect to n_a and combine it with Eq. (2). We can obtain the RI sensitivity, which is expressed by

$$\frac{d\lambda}{dn_a} = \frac{\lambda}{G(\lambda, n_a)} \frac{\partial B(\lambda, n_a)}{\partial n_a}. \tag{4}$$

For two adjacent transmission dips in the interference spectrum with wavelength spacing of $\Delta\lambda$, the accumulated phase difference over $\Delta\lambda$ is $\pm 2\pi$, from which we can deduce that the absolute value of group birefringence |G| can be determined as follows:

$$|G| = \lambda^2/(\Delta\lambda L). \tag{5}$$

In order to numerically study the spectral properties and RI response of the proposed microfluidic Sagnac interferometer, we use a full-vector finite-element method to simulate the mode properties of the PM-PCF filled with analytes with different RI values. We use the commercially available COMSOL software to solve wave equations and calculate the effective indices of the guided modes of the PM-PCF. Through wavelength scanning, i.e., performing simulations at different wavelengths, we achieve the values of phase modal birefringence B as a function of wavelength. Then we do the third-order polynomial fitting for B and λ so that we can calculate the derivative of B with respect to λ. And then according to Eq. (2) we calculate the value of group modal birefringence G. The simulation results of B and G as a function of λ for air-filled ($n_a = 1.0$) and water-filled ($n_a = 1.333$) PM-PCF are plotted in Fig. 2(a). It is observed that at the wavelength of 1550 nm, the values of G of the PM-PCF before and after water filling are -8.0×10^{-4} and -3.1×10^{-4}, respectively. In the simulation, the material dispersion of silica and water are considered according to the Sellmeier equation [19].

To calculate the theoretical value of the RI sensitivity of our sensor, we set n_a with different values and repeat the previous wavelength scanning process at each n_a value. Hence we can obtain the curves of B as a function of λ at different n_a values. By substituting the obtained $B(\lambda, n_a)$ to Eq. (1), the simulated output spectra for different n_a values are obtained and plotted in Fig. 3(a). Then the RI sensitivity can be calculated by tracking the spectral shift of Fig. 3(a). Alternatively, from above simulation results, one can also obtain the value of $\partial B/\partial n_a$ for a specific λ and then calculate the RI sensitivity according to Eq. (4). These two methods give the same sensitivity since they are both deduced from Eq. (1). The calculated RI sensitivities are 5116 nm/RIU and 5385 nm/RIU for the wavelengths of 1550 and 1620 nm, respectively. In Eq. (4), both the terms of G and $\partial B/\partial n_a$ are negative, resulting in positive RI sensitivity. This indicates that the spectrum redshifts with increase in n_a, which is consistent with Fig. 3(a).

Experiments are carried out to verify the theoretical predictions. One of the SMF-C-PCF joints is immersed in a bath filled with de-ionized (DI) water. Due to the capillary force [20], the DI water automatically fills the microfluidic channels of the PM-PCF. Since the water-filled PM-PCF has lower group modal birefringence, the wavelength spacing of the interference spectrum becomes larger and larger during water filling. After 6 min, the spectral evolution stops, indicating that the water is fully filled over the entire length of the PM-PCF. Figure 2(b) shows the output spectra of the Sagnac interferometer before and after water filling. The wavelength spacing of the spectra for air- and water-filled PM-PCF is 24.82 and 74.10 nm, respectively. According to Eq. (5), the absolute value of G is calculated to be 8.41×10^{-4} and 2.97×10^{-4} for the two cases, which agrees well with the theoretical value in Fig. 2(a).

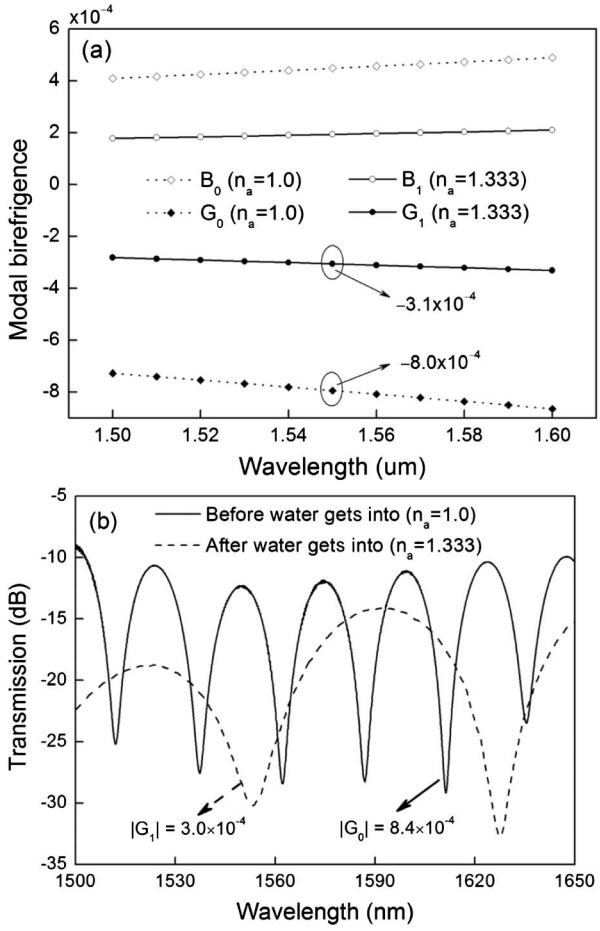

Fig. 2. (a) Simulation of modal birefringence of PM-PCF before and after water filling. (b) Output spectra before and after water filling at room temperature.

The PM-PCF Sagnac interferometer is intrinsically temperature insensitive because it is made of pure silica [17]. Therefore, one can tune the RI of the water filled in the PM-PCF through temperature change [19] and then characterize its capability of detecting small RI change. After the PM-PCF is fully filled with water, we immerse the entire SMF-C-PCF-C-SMF device into the water bath, and then change the temperature of the water bath. A FLUKE 52II thermometer with accuracy of 0.1°C is used to monitor the temperature change. Figure 3(b) shows the spectral shift for different values of n_a, i.e., at different temperatures. As can be seen from it, with increase in n_a, the spectrum shifts to longer wavelength. Both the trend and amplitude of the spectral shift are consistent

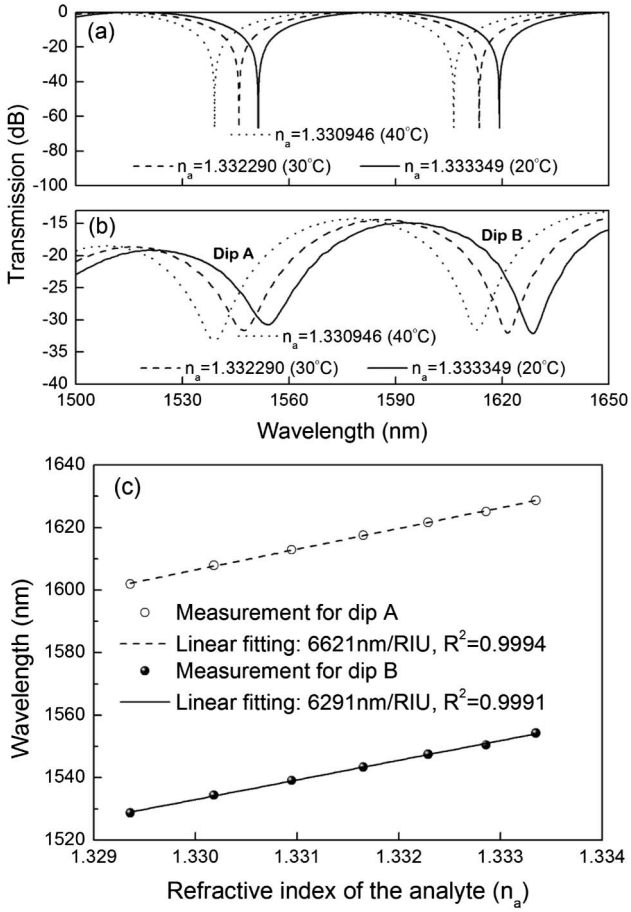

Fig. 3. (a) Simulated spectrum shift. (b) Measured spectrum shift. (c) Measured wavelength shift as a function of n_a.

with the theoretical results presented in Fig. 3(a). In the simulation, the transmission loss is not taken into account, leading to degradation on the fringe visibility for the experimental results. Nevertheless, we focused on the wavelength shift behavior of the spectrum.

Figure 3(c) shows the wavelength shift as a function of n_a for the two transmission dips labeled in Fig. 3(b). Through linear fitting, we find the RI sensitivity at 1550 and 1620 nm wavelength ranges are 6291 and 6621 nm/RIU, respectively. The R^2 value is better than 0.999. The measured RI sensitivity is a little larger than the theoretical value. The small discrepancy is probably due to inaccurate RI data of water used in the simulation. In [19], the equation for the RI of water as a function of wavelength is only valid in the visible wavelength range. It suffers some error in the infrared wavelength range. In the experiment, we used an AQ6370 OSA with resolution of 0.02 nm to measure the interference spectrum. Therefore, the RI detection limit is calculated to be 5.2×10^{-6} according to [21,22].

In conclusion, we have demonstrated a highly sensitive in-line microfluidic refractometer based on an SMF-C-PCF-C-SMF structure formed Sagnac interferometer. The entire fabrication process only involves fusion splicing and thus is cost effective. Over the RI range from 1.330 to 1.333, it exhibits high sensitivity of 6621 nm/RIU with good linearity. It is potentially attractive in the context of biosensing where detection of small RI change in aqueous environment is highly desired.

This work is supported in part by the China National Funds for Distinguished Young Scientists under grant 61225023, in part by the Fundamental Research Funds for the Central Universities under grant 1613334, and in part by the Hong Kong Polytechnic University under grant 4-ZZE4.

References

1. X. D. Fan, I. M. White, S. I. Shopova, H. Y. Zhu, J. D. Suter, and Y. Z. Sun, Anal. Chim. Acta **620**, 8 (2008).
2. X. W. Shu, L. Zhang, and I. Bennion, J. Lightwave Technol. **20**, 255 (2002).
3. W. Liang, Y. Y. Huang, Y. Xu, R. K. Lee, and A. Yariv, Appl. Phys. Lett. **86**, 151122 (2005).
4. C. Monat, P. Domachuk, and B. J. Eggleton, Nat. Photonics **1**, 106 (2007).
5. X. D. Fan and I. M. White, Nat. Photonics **5**, 591 (2011).
6. J. M. Fini, Meas. Sci. Technol. **15**, 1120 (2004).
7. J. B. Jensen, L. H. Pedersen, P. E. Hoiby, L. B. Nielsen, T. P. Hansen, J. R. Folkenberg, J. Riishede, D. Noordegraaf, K. Nielsen, A. Carlsen, and A. Bjarklev, Opt. Lett. **29**, 1974 (2004).
8. S. Unterkofler, R. J. McQuitty, T. G. Euser, N. J. Farrer, P. J. Sadler, and P. St. J. Russell, Opt. Lett. **37**, 1952 (2012).
9. S. Kassani, J. Park, Y. Jung, J. Kobelke, and K. Oh, Opt. Express **21**, 14074 (2013).
10. M. C. P. Huy, G. Laffont, V. Dewynter, P. Ferdinand, P. Roy, J. L. Auguste, D. Pagnoux, W. Blanc, and B. Dussardier, Opt. Lett. **32**, 2390 (2007).
11. L. Rindorf and O. Bang, Opt. Lett. **33**, 563 (2008).
12. D. K. C. Wu, B. T. Kuhlmey, and B. J. Eggleton, Opt. Lett. **34**, 322 (2009).
13. C. M. B. Cordeiro, C. J. S. de Matos, E. M. dos Santos, A. Bozolan, J. S. K. Ong, T. Facincani, G. Chesini, A. R. Vaz, and C. H. B. Cruz, Meas. Sci. Technol. **18**, 3075 (2007).
14. Y. Liu, B. Liu, X. Feng, W. Zhang, G. Zhou, S. Yuan, G. Kai, and X. Dong, Appl. Opt. **44**, 2382 (2005).
15. W. W. Qian, C. L. Zhao, S. He, X. Dong, S. Zhang, Z. Zhang, S. Jin, J. Guo, and H. Wei, Opt. Lett. **36**, 1548 (2011).
16. X. B. Zheng, Y. G. Liu, Z. Wang, T. T. Han, C. L. Wei, and J. J. Chen, Appl. Phys. Lett. **100**, 141104 (2012).
17. C. L. Zhao, X. Yang, C. Lu, W. Jin, and M. S. Demonkan, IEEE Photon. Technol. Lett. **16**, 2535 (2004).
18. M. L. V. Tse, H. Y. Tam, L. B. Fu, B. K. Thomas, L. Dong, C. Lu, and P. K. A. Wai, IEEE Photon. Technol. Lett. **21**, 164 (2009).
19. A. H. Harvey, J. S. Gallagher, and J. M. H. L. Sengers, J. Phys. Chem. Ref. Data **27**, 761 (1998).
20. K. Nielsen, D. Noordegraaf, T. Sørensen, A. Bjarklev, and T. P. Hansen, J. Opt. A **7**, L13 (2005).
21. I. M. White and X. D. Fan, Opt. Express **16**, 1020 (2008).
22. Y. Wang, M. Yang, D. N. Wang, S. Liu, and P. Lu, J. Opt. Soc. Am. B **27**, 370 (2010).